CMS Physics Analysis Summary

Contact: cms-pag-conveners-susy@cern.ch 2011/10/26

Searches for Supersymmetry using Multilepton Signatures in pp Collisions at 7 TeV

The CMS Collaboration

Abstract

A search for physics beyond the standard model using events with at least three leptons is presented. The data sample corresponds to 2.1 fb^{-1} of integrated luminosity in pp collisions at $\sqrt{s} = 7$ TeV collected by the CMS experiment at the LHC. Standard model backgrounds are suppressed by requiring missing transverse energy, invariant mass of lepton pairs inconsistent with that of the Z boson, or high jet activity. Control samples in data are used to ascertain the robustness of background evaluation techniques and to minimize the reliance on simulation. The observations are mostly consistent with expectations from standard model processes. These results are used to exclude previously unexplored regions of the supersymmetric parameter space assuming R-parity conservation with the lightest supersymmetric particle being either a neutralino or gravitino.

1 Introduction

Supersymmetry (SUSY) is a well known candidate for a theory beyond the standard model (SM) because it solves the hierarchy problem, allows the unification of the gauge couplings, and may provide a candidate particle for dark matter [1–3]. Hadronic collisions yielding three or more electrons, muons, or tau leptons (defining the "multilepton" signature) serve as an ideal hunting ground for physics beyond the SM, as leptonic SM processes are relatively rare at hadron colliders.

Using 2.1 fb^{-1} of LHC data collected with the Compact Muon Solenoid (CMS) detector at a centre of mass energy of 7 TeV, we probe multiple new regions of the supersymmetric parameter space not yet excluded by previous multilepton searches [4–11]. The analysis described in this paper is similar in structure to our previous analysis [11], but uses substantially larger integrated luminosity. Although the search is not tailored to any particular SUSY scenario, we use its results to study scenarios with neutralinos as well as gravitinos as the stable lightest supersymmetric particle (LSP) assuming R-parity conservation. If the neutralino is the LSP the results are analyzed in the context of the CMSSM [12, 13] scenario in which the superpartner masses and gauge couplings become unified at the grand unification scale, resulting in common masses m_0 ($m_{1/2}$) for all spin 0 (1/2) superpartners at this scale. The remaining CMSSM parameters are A_0, $\tan\beta$, and the sign of μ. If the gravitino is the LSP, the sleptons are assumed to be the next-to-lightest supersymmetric particles (NLSPs). Scenarios of this type arise in a wide class of theories of gauge mediation with split messengers (GMSM) [14, 15]. Multilepton final states arise naturally in the subset of the GMSM parameter space where the right-handed sleptons are flavor-degenerate, the so-called slepton co-NLSP scenario [6, 14–16].

2 Detector and Simulation

The data sample used in this search corresponds to an integrated luminosity of 2.1 fb^{-1} recorded in 2011 with the CMS detector at the LHC. The CMS detector has cylindrical symmetry around the pp beam axis with tracking and muon detector pseudorapidity coverage to $|\eta| < 2.4$, where $\eta = -\ln\tan(\theta/2)$ and θ is the polar angle with respect to the counterclockwise beam. The azimuthal angle ϕ is measured in the plane perpendicular to the beam direction. Charged particle tracks are identified with a 200 m^2, fully silicon-based tracking system composed of a pixel detector with three barrel layers at radii between 4.4 cm and 10.2 cm and a silicon strip tracker with 10 barrel detection layers, of which four are double sided, extending outwards to a radius of 1.1 m. Each system is completed by endcaps extending the acceptance of the tracker up to a pseudorapidity of $|\eta| < 2.5$. The lead-tungstate scintillating crystal electromagnetic calorimeter and brass/scintillator hadron calorimeter hermetically surrounding the tracking system measure the energy of showering particles with $|\eta| < 3.0$. These subdetectors are placed inside a 13 m long and 6 m diameter superconducting solenoid with a central field of 3.8 T. Outside the magnet is the tail-catcher of the hadronic calorimeter followed by the instrumented iron return yoke, which serves as a multilayered muon detection system in the range $|\eta| < 2.4$. The CMS detector has extensive forward calorimetry, extending the pseudorapidity coverage to $|\eta| < 5.0$. The performance of all detector components as measured with cosmic rays has been reported in Ref. [17] and references therein. A much more detailed description of CMS can be found elsewhere [18].

All detector simulations were performed with GEANT4 [19]. The important SM backgrounds for this analysis (Z/γ^* + jets, $t\bar{t}$ quark pairs, and double vector boson production) were gen-

erated using MADGRAPH [20]; QCD events were generated with PYTHIA 8.1 [21]. We use the CTEQ6.6 parton distribution functions [22]. For the dominant WZ+jets contribution up to two jets were selected at the matrix element level in MADGRAPH. The two-jet contribution, although of higher order in the coupling constant of QCD, is still comparable to the zero and one jet contribution, because even for a single quark flavor more than 2000 diagrams contribute at leading order.

The data used for this search came from single and double-lepton triggers. The trigger thresholds were different for the different triggers. Single lepton triggers have a p_{T} threshold of 17 and 65 GeV for muons and electrons, respectively. The double-muon trigger has a p_{T} cut-off of 13(7) GeV, the double electron trigger of 17(8) GeV, the $e\mu$ trigger 8(17) GeV/c and the μe trigger 8(17) GeV, where the number in parenthesis is the threshold for the second lepton in the trigger. The trigger efficiencies are measured directly using a data sample independently triggered by the sum of hadronic energy in jets (H_T), assuming no correlations between these and the signal triggers. The two most important double-electron and double-muon trigger have efficiencies of 99$\pm$2% and 93 $\pm$ 3%, respectively. The single-electron and single-muon trigger are less significant for this search and have efficiencies of 96$\pm$1% and 92.0 $\pm$ 0.5%, respectively. We scale each simulated event by the probability for it to satisfy either the single-lepton or the double-lepton triggers. The uncertainty in the correction to the simulation translates into a systematic uncertainty in the irreducible backgrounds and signal efficiencies.

3 Lepton Identification

Leptons in this search can be either electrons, muons, or tau leptons. We use electrons and muons with $p_{\mathrm{T}} \geq 8$ GeV and $|\eta| < 2.1$. They are reconstructed from measured quantities from the tracker, calorimeter, and muon system. The matching candidate tracks must satisfy quality requirements and spatially match with the energy deposits in the electromagnetic calorimeter and the tracks in the muon detectors, as appropriate. Details of reconstruction and identification can be found in Ref. [23] for electrons and in Ref. [24] for muons. Jets are reconstructed using particles with $|\eta| \leq 2.5$ via the particle-flow (PF) algorithm [25].

τ leptons can decay either leptonically (τ_ℓ) to electrons or muons in which case they are selected as such; or hadronically (τ_h). The hadronic decays yield either a single charged track (one-prong) or three charged tracks (three-prong) with or without additional electromagnetic energy from neutral pion decays. In this analysis, we use only one-prong hadronic τ decays. Two selections are made: the track can have either no electromagnetic energy (expected e.g. from $\tau \to \pi\nu_\tau$ decay) or it has electromagnetic energy in a narrow cone of $\Delta R < 0.1$ around the track (expected e.g. from $\tau \to \rho\nu_\tau$ decay). For the track without electromagnetic energy we require $p_{\mathrm{T}} > 8$ GeV. For the track with electromagnetic energy we require the invariant mass of the track and electromagnetic energy to be consistent with the visible mass expected from hadronic τ decays, and the visible p_T of the hadronic τ candidate to be greater than 15 GeV. The last requirement ensures that the τ's are in a kinematic region where the reconstruction efficiency is well understood.

An isolation requirement strongly reduces the background from misidentified leptons, since most of them occur inside jets, like e.g. leptons from punch-through into the muon system, hadronic showers with large electromagnetic fractions, or photon conversions. For muons and isolated tracks, we require $I_{\mathrm{rel}} < 0.15$, where the relative isolation I_{rel} is defined as the ratio of the sum of calorimeter energy and p_{T} of any other tracks in the cone defined by

$\Delta R = \sqrt{(\Delta\eta)^2 + (\Delta\phi)^2} < 0.3$ around the candidate lepton to the p_{T} of the lepton. The same requirement applies to the electron, but with the cone size of 0.4. For the isolation of the hadronic tau decays including electromagnetic energy the calorimeter tower E_T is summed in an annulus of $0.1 < R < 0.3$ around the isolated track. The isolation parameter I_{rel} in this case is the isolation energy divided by the visible p_{T} of the τ candidate. For all leptons, in addition to the I_{rel} requirement, the sum of calorimeter energy and track p_{T} can not exceed 10 GeV.

Leptons from SUSY decays considered in this search originate from the collision point ("prompt" leptons). After the isolation selection, the most significant background sources are residual non-prompt leptons from heavy quark decays, where the lepton tends to be more isolated because of the high p_{T} with respect to the jet axis. This background is reduced by requiring that the leptons originate from within one centimeter of the primary vertex in z and that the impact parameter d_{xy} between the track and the event vertex in the plane transverse to the beam axis be small: $d_{xy} \leq 0.02$ cm. The isolation and promptness criteria would retain the SUSY signal of prompt leptons, but restrict the background from misidentified leptons to the signal region defined by $I_{\mathrm{rel}} < 0.15$ and $d_{xy} \leq 0.02$ cm.

4 Search Strategy

Candidate events in this search must have at least three leptons, of which at least one must be an electron or a muon. The thresholds on the transverse momenta of the leptons are chosen such that triggers used are maximally efficient on these events. Events satisfying any of the following lepton requirements are selected:

- for single lepton triggers: a leading muon (electron) with $p_T > 20(70)$ GeV;
- for same-flavor dilepton triggers: a leading muon (electron) with $p_T > 15(20)$ GeV and a next to leading muon(electron) with $p_T > 10(10)$GeV;
- for different-flavor dilepton triggers: a leading muon (electron) with $p_T > 20$ GeV and a leading electron (muon) with $p_T > 10$ GeV.

We classify multilepton events into search channels on the basis of the number of leptons, lepton flavor, and relative charges as well as charge and flavor combinations and other kinematic quantities described below. In describing pairs of leptons, OS stands for opposite-sign, SS for same-sign, and SF for same (lepton) flavor. To explicitly denote different lepton flavors in a pair, we use the symbol $\ell\ell'$, where the symbol ℓ stands for an electron or a muon.

For multilepton searches, the SM background is small and can be further reduced by minimal requirements on either hadronic activity or missing energy above the typical SM values. The presence of hadronic activity in an event is characterized by the variable H_{T}, defined as the scalar sum of the transverse jet energies for all jets with $E_{\mathrm{T}} > 40$ GeV. Jets used for the H_{T} determination must be well separated from any identified leptons; jets are required to have no isolated lepton in a cone $\Delta R < 0.3$ around the jet axis. The missing transverse energy, $E_{\mathrm{T}}^{\mathrm{miss}}$, is defined as the magnitude of the vectorial sum of the momenta of all candidate particles reconstructed with CMS's Particle Flow [25] algorithm. Comparison between data and simulation shows good modeling of $E_{\mathrm{T}}^{\mathrm{miss}}$ [26, 27] and is valid for our particular selection and data collecting period as well, as will be shown later.

Both H_{T} and $E_{\mathrm{T}}^{\mathrm{miss}}$ are good discriminating observables for physics beyond the SM, as demonstrated in Fig. 1. The signal expectations for two benchmark points are shown as well. The CMSSM benchmark point, called "TeV3", is characterized by $m_0 = 60\,\mathrm{GeV}/c^2$, $m_{1/2} = 230\,\mathrm{GeV}/c^2$,

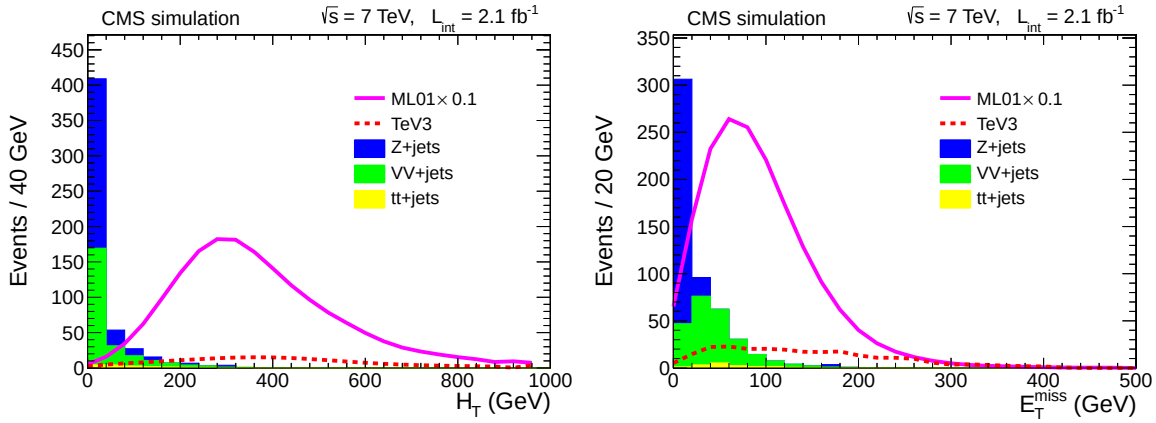

Figure 1: The H_{T} (left) and $E_{\mathrm{T}}^{\mathrm{miss}}$ (right) distributions for SM background channels (Z+jets, $\mathrm{t\bar{t}}$, and VV+jets, where V = W, Z, and two SUSY benchmark points for the simulated events that pass all other requirements for the three-lepton events. The ML01 and TeV3 benchmark points are defined in the text.

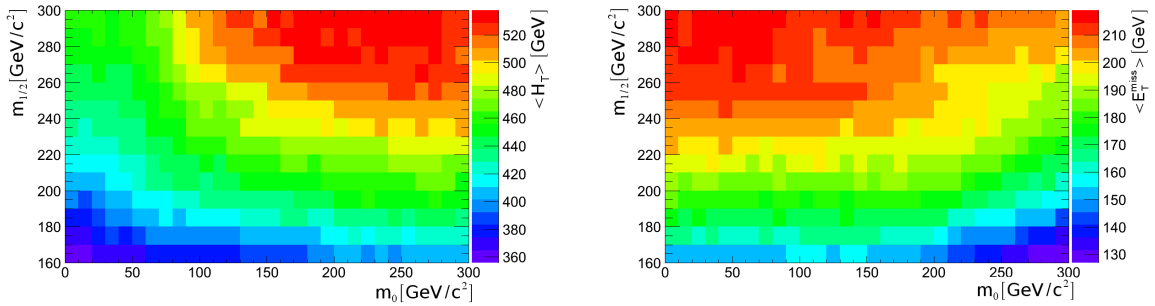

Figure 2: Average H_{T} and $E_{\mathrm{T}}^{\mathrm{miss}}$ in the CMSSM (m_0,$m_{1/2}$) plane for fixed $\tan\beta = 3$ and $A_0 = 0$.

$A_0 = 0, \tan\beta = 3, \mu > 0$ and a next-to-leading order (NLO) total production cross section of 10 pb. The co-NLSP benchmark point, called ML01, is characterized by a chargino mass $m_{\chi^{\pm}} = 385\,\mathrm{GeV}/c^2$ and gluino mass $m_{\tilde{g}_L} = 450\,\mathrm{GeV}/c^2$. The other superpartner masses are then given by the generic relationships $m_{\tilde{\ell}_R} = 0.3m_{\chi^{\pm}}, m_{\chi_1^0} = 0.5m_{\chi^{\pm}}, m_{\tilde{\ell}_L} = 0.8m_{\chi^{\pm}}$, and $m_{\tilde{q}_L} = 0.8m_{\tilde{g}_L}$. ML01 has an estimated 45 pb NLO total production cross section. In specific regions of parameter space one discriminating observable may be more effective than the other. This is demonstrated for the CMSSM model in Fig. 2. In order to retain search sensitivity for as broad a region of new physics as possible both $E_{\mathrm{T}}^{\mathrm{miss}}$ and H_{T} selections have been used.

We exploit the background reduction ability of both $E_{\mathrm{T}}^{\mathrm{miss}}$ and H_{T} as follows [11]. Events with $E_{\mathrm{T}}^{\mathrm{miss}} > 50\,\mathrm{GeV}$ ($H_{\mathrm{T}} > 200\,\mathrm{GeV}$) are said to satisfy the $E_{\mathrm{T}}^{\mathrm{miss}}$ (H_{T}) requirement. The justification for the values chosen is evident from Fig. 1. These variables are well described by the simulation, as shown in Fig. 3 for events with two isolated and one lepton with isolation selection removed.

Another criterion for background reduction is the "Z veto", in which the invariant mass of the OSSF lepton pairs is required to be outside the 75–105 GeV/c^2 window. Events with OSSF lepton pairs must have $M(2\ell) > 12$ GeV/c^2 for all combinations in order to reject low mass Drell–Yan production and the J/ψ(1S) and Υ resonances. A possible source of background is from the final state radiation (FSR) in $\mathrm{Z} \to 2\ell(\ell = e, \mu)$ events with a $\gamma \to 2\ell$ conversion and

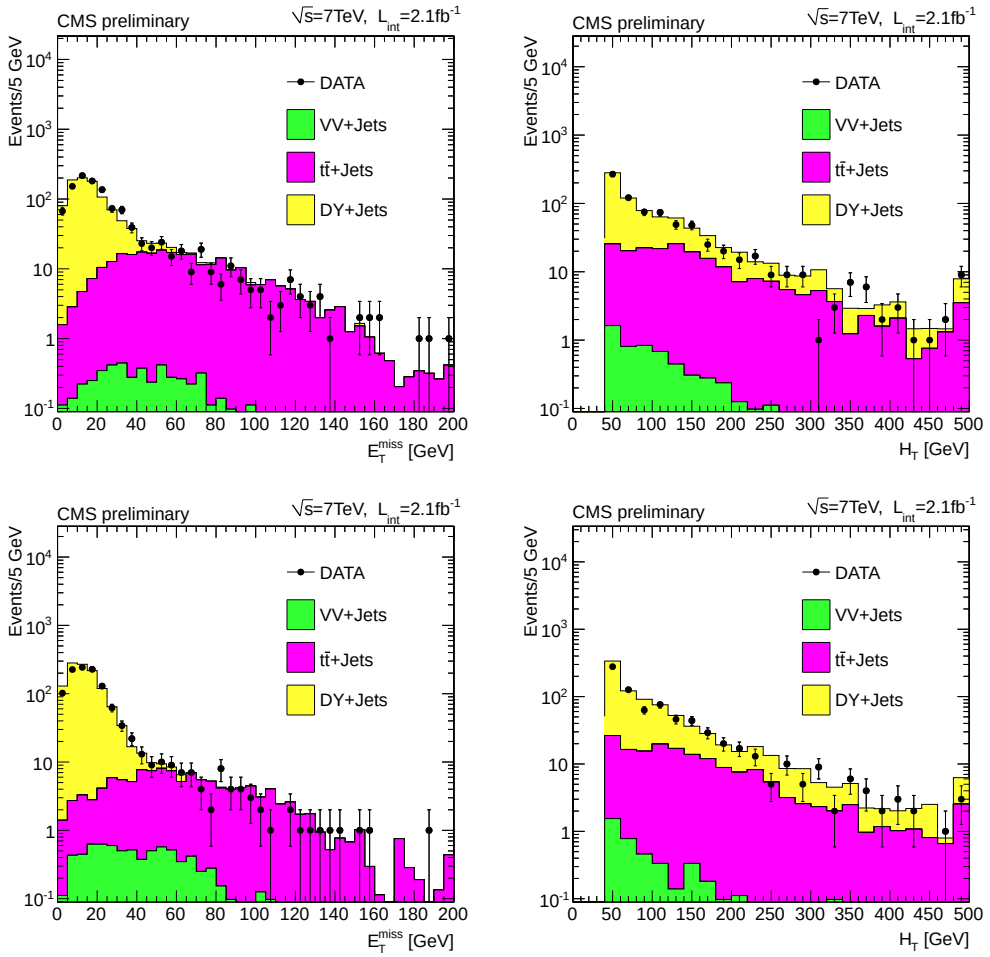

Figure 3: $E_{\mathrm{T}}^{\mathrm{miss}}$ (left)and H_{T} (right) distributions for $\ell\ell - \mu$ (top), $\ell\ell - e$ (bottom), where two leptons $\ell\ell$ are isolated but the third lepton is required to be non-isolated. VV, TT and DY refers to the diboson, top-quark and Drell-Yan SM production, respectively.

one lepton failing to pass the selection criteria. Therefore, the Z veto requirement is applied to the invariant mass $M(3\ell)$ of three leptons universally. The contribution of FSR will be discussed in more detail below, when we discuss a data driven technique for estimating this background.

In total 52 multilepton channels have been investigated with subdivisions based on the presence of hadronic energy ($H_{\mathrm{T}} > 200$ or $H_{\mathrm{T}} < 200$ GeV) or missing transverse energy ($E_{\mathrm{T}}^{\mathrm{miss}} > 50$ or $E_{\mathrm{T}}^{\mathrm{miss}} < 50$ GeV) and the presence of an OSSF pair near the Z mass. The kinematic properties of the event determine the extent of SM background for a given channel.

5 Background Estimation

5.1 Background from misidentified leptons

The largest background remaining after the basic three-lepton reconstruction originates from the Z+jets process (including Drell-Yan production), in which the Z boson decays leptonically and a third misidentified lepton is produced from a jet in the event. Since the QCD component in such processes is difficult to simulate, we use data to estimate backgrounds from $Z + \text{jets} \rightarrow$

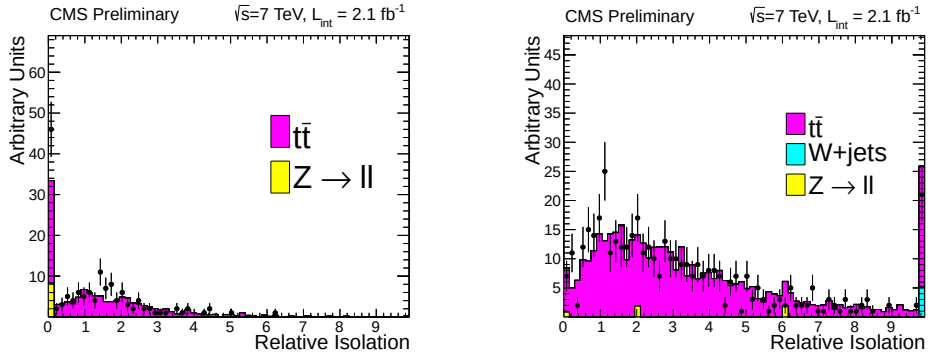

Figure 4: The isolation distribution of electrons (left) and muons (right) with large impact parameter ($d_{xy} > 0.02$ cm, primarily from jets) in a data sample enriched in $t\bar{t} \to \ell\nu bbjj$. The last bin includes the sum of all bins above this bin. The number of non-prompt isolated muons is 7, with an MC expectation of 7.5 ± 1.0.

2ℓ, as well as for $W^+W^- \to 2\ell +$ jets, and other $N_\ell < 3$ processes.

The probability that an isolated track is misidentified as a lepton is measured in control samples where no signal is present, such as in dijet samples. We measure the probability for an isolated track to produce a misidentified muon (electron) to be $1.4\% \pm 0.2\%$ ($1.1\% \pm 0.2\%$). The misidentification rate in events with three leptons is obtained by multiplying the number of isolated tracks in the sample with two leptons by this probability. In a similar way we estimate the misidentified background for four-lepton events by examining two-lepton events with two isolated tracks. The systematic uncertainty on this rate originates from the difference in jet environment in QCD and Z+jets control samples. Such differences are expected to arise from the variation of heavy quark content across the control samples and are accounted for by determining the misidentification rate as function of the impact parameter distribution.

For channels with τ_h reconstructed as isolated track, we extrapolate the isolation sideband $0.2 < I_{\text{rel}} < 1.0$ to the signal region $I_{\text{rel}} < 0.15$. The ratio of the number of isolated tracks in the two regions is $(15 \pm 3)\%$. We study the variation of this ratio for a number of QCD samples and assign a 30% systematic uncertainty for it. The ratio is applied to the 2ℓ event sample.

Our misidentification rate determination has been cross checked by two independent methods. First, we use simulation of the underlying processes to estimate the background after verifying the simulation in control regions devoid of possible signals. For this we use sidebands of the isolation parameter and scale the simulation to agree with the data in the sidebands of control regions for each underlying process. The scaling factors are consistent with one for all underlying processes, indicating that the simulation describes the data well, as indicated before in Fig. 3 and so simulation can be used to estimate the background rate from SM processes.

Instead of extrapolating from the isolation sideband one can also extrapolate in the two-dimensional isolation versus impact parameter plane, if one assumes these two variables I_{rel} and d_{xy} are uncorrelated, so both can be independently extrapolated. These two independent cross checks gave consistent results with the data driven method discussed above.

5.2 Background from $t\bar{t}$ Production

This background is estimated from simulation after careful validation in the single lepton control region enriched to be primarily $t\bar{t}$. The single lepton control region requires one isolated

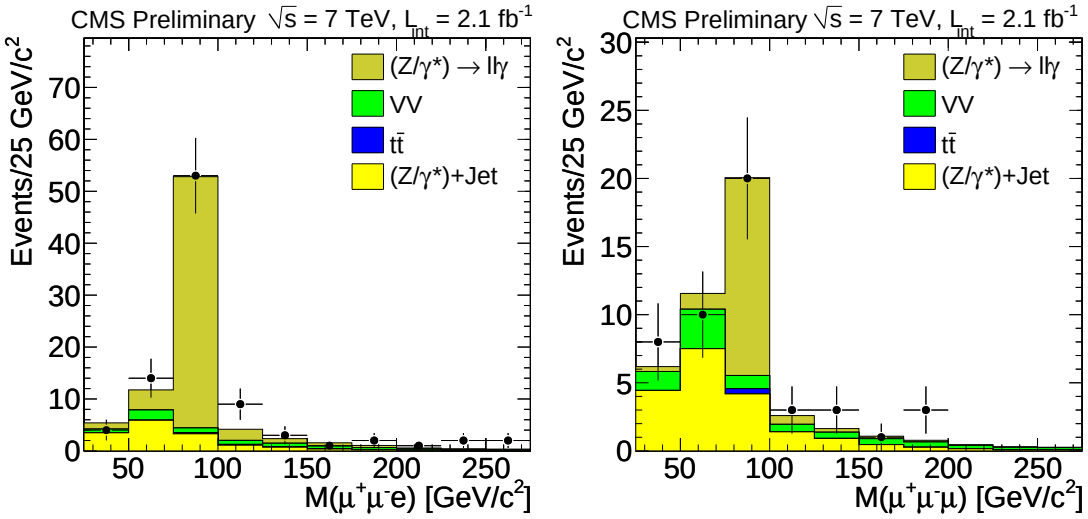

Figure 5: Trilepton invariant mass distributions after all other selections. Left: $\mu^+\mu^-$e channel; right: $\mu^+\mu^-\mu$ channel. Of note is the substantial Z peak in the $\mu^+\mu^-\mu$ channel due to the *internal* conversion process $\gamma^* \to \mu^+\mu^-$ where one of the muons is lost, as discussed in the text.

muon with $p_T > 30$ GeV or electron with $p_T > 70$ GeV, at least 3 jets, one of which must satisfy a high efficiency b-tag. Fig. 4 shows the relative isolation of additional non-isolated leptons in the single lepton control region in comparison with the simulation. Despite limited statistics, a good agreement between data and simulation, both in shape and normalization, is observed.

5.3 Irreducible Background from WZ production

The SM can produce 3 or more real, prompt leptons with $E_{\mathrm{T}}^{\mathrm{miss}}$ or H_{T} via diboson+jets production where both bosons decay leptonically. This class of background is referred to as "irreducible" because its characteristics are too similar to the search signature. Since this background cannot be predicted directly from the data without invoking specific signal models, it must be obtained from theory and Monte Carlo simulations. However, one can check the simulation against control samples. We verify the simulation by comparing with data samples enriched in WZ-production, the dominant contribution to trilepton signatures from diboson+jets. WZ samples can be selected by requiring three leptons, $E_{\mathrm{T}}^{\mathrm{miss}}$, and an on-shell Z. The simulation describes such a pure sample of WZ events well within the statistical uncertainty of 15%, so no rescaling of the simulation is needed to estimate the irreducible background.

5.4 Backgrounds From Asymmetric Photon Conversions

There are two different types of photon conversions that can give rise to backgrounds in multilepton analyses. The first type is an "external conversion" into an $\ell^+\ell^-$ pair in the external magnetic field or material of the detector. This conversion is predominantly into e^+e^- pairs. The second type of photon conversions are "internal conversions", also known as Dalitz decays, where the photon is virtual and can produce muons almost as often as electrons. In case of asymmetric conversions, where one lepton does not pass the selection criteria, Drell-Yan processes with such conversions can lead to a significant background for three lepton signatures. Events with asymmetric conversion can be studied from data, since in this case the 3-body invariant mass of the $\ell^+\ell^-\ell$ will be close to the Z mass. Fig. 5 shows the invariant mass of the three leptons in events where no OSSF dilepton pair forms an invariant mass of the

Channel	$\ell\ell + Jet$	$\ell\ell + \gamma$	$t\bar{t}$	VV	Total SM	Data	Signal
$OS(\ell\ell)e$	0.33±0.08	0.42±0.42	1.5±0.8	3.3±1.3	6.0±1.7	10	76±19
$OS(\ell\ell)\mu$	0.42±0.10	0.17±0.17	2.2±1.1	4.3±1.7	7.5±2.1	14	106±21
$OS(\ell\ell)\tau$	28.4±4.4	0.35±0.35	29±15	4.5±1.7	63±16	71	202±30
$\ell\ell'\tau$	24.6±6.0	1.7±1.7	38±19	7.5±2.9	73±20	88	29±10
$SS(\ell\ell)\ell'$	0.45±0.08	0.35±0.35	2.3±1.1	0.49±0.18	4.3±1.3	6	9.1±5.4
$SS(\ell\ell)\tau$	3.9±1.5	0.48±0.48	1.7±0.9	3.4±1.3	9.9±2.3	21	4.0±4.0
$\ell\tau\tau$	96±18	NA	12.3±6.2	1.7±0.6	110±19	88	24.0±9.1
$\sum \ell(\ell/\tau)(\ell/\tau)$	154±28	3.1±3.1	87±44	25.3±9.7	273±53	298	450±49
$\ell\ell\ell\ell$	0.0000±0.0006	<0.0002	<0.006	0.016±0.005	0.016±0.006	1	14.6±7.4
$\ell\ell\ell\tau$	0.00±0.07	<0.007	<0.07	0.14±0.04	0.23±0.11	0	14.8±7.7
$\ell\ell\tau\tau$	0.34±0.33	<0.005	0.27±0.13	0.14±0.04	0.89±0.40	0	7.8±5.6
$\sum \ell\ell(\ell/\tau)(\ell/\tau)$	0.34±0.34	0.00±0.00	0.27±0.13	0.29±0.08	1.14±0.42	1	37±12

Table 1: Summary of multilepton observations and expectations by lepton flavor for 2.1 fb^{-1} of luminosity with MET $>$ 50 GeV requirement. Events with Z candidates have been removed.

Z boson. Contributions from various processes including conversions are also shown. Note the different contributions for electrons and muons. For electrons the third electron originates from radiation from the final state electrons. Since muons hardly radiate and external conversions rarely yield muons, the main contribution originates from internal pair conversion at the matrix element level. We do not use Monte Carlo approach for this background because the simulation of such asymmetric internal conversions at the matrix element level is difficult and so is the path-tracing of the conversion pair through the detector that follows. This motivates data-based measurements of the photon to e/μ conversion factors, measured assuming the rate for the production of on-shell photons and virtual photons yielding asymmetric conversions to be proportional to each other. We measure the conversion factors in a control region devoid of new physics (low $E_{\mathrm{T}}^{\mathrm{miss}}$ and low H_{T}). The ratio of the number of $\ell^+\ell^-\ell^\pm$ on the Z peak to the number of $\ell^+\ell^-\gamma$ on the Z peak defines the conversion factor, which is $0.35\% \pm 0.1\%$ ($1.1\% \pm 0.2\%$) for muons (electrons). The uncertainties are statistical only. We assign systematic uncertainties of 100% to these conversion factors from our underlying assumption of proportionality between virtual and on-shell photons. The measured conversion factors are then used to estimate the background in the signal regions from the observed number of $\ell^+\ell^-\gamma$ events in the signal regions. The background contribution from these converted photons is small after the final selection cuts, as will be shown in the next section.

6 Results and their Interpretation

Tables 1 and 2 show the expected and observed numbers of three- and four-lepton events after the $E_{\mathrm{T}}^{\mathrm{miss}}$ and H_{T} requirements, respectively. The different SM background contributions and the expected number of signal events for the TeV3 CMSSM point ($m_0 = 60$, $m_{1/2} = 230$, tanβ = 3, $A_0 = 0$) are shown as well [11]. One observes that the SM background for the $H_{\mathrm{T}} > 200$ GeV is considerably smaller than for the $E_{\mathrm{T}}^{\mathrm{miss}} > 50$ GeV requirement, as expected already from Fig. 1. Table 3 shows the same observations with additional control regions, namely the non-signal regions with $E_{\mathrm{T}}^{\mathrm{miss}} < 50$ GeV and/or $H_{\mathrm{T}} < 200$ GeV combined with or without a Z candidate in the event. Furthermore, the channels are classified according to the number of τ candidates (columns), which shows the larger background for events including hadronic τ decay candidates. The observed number of events in the channels we examine is largely consistent with expectations. We show characteristics of 3ℓ events which comprise the classic

Channel	$\ell\ell + Jet$	$\ell\ell + \gamma$	$t\bar{t}$	VV	Total SM	Data	Signal
$OS(\ell\ell)e$	0.21±0.06	0.5±0.5	0.14±0.07	0.68±0.26	1.8±0.6	8	56±15
$OS(\ell\ell)\mu$	0.26±0.07	0.21±0.21	0.63±0.31	0.88±0.34	2.1±0.6	2	87±19
$OS(\ell\ell)\tau$	28.5±4.3	0.25±0.25	7.8±3.9	0.98±0.37	37.4±5.8	31	154±26
$\ell\ell'\tau$	3.6±1.6	0.6±0.6	12.3±6.2	1.6±0.6	18.6±6.6	29	25.6±9.8
$SS(\ell\ell)\ell'$	0.18±0.05	0.06±0.07	0.55±0.27	0.13±0.05	1.06±0.38	3	6.7±4.7
$SS(\ell\ell)\tau$	2.0±0.9	0.24±0.25	0.23±0.12	0.72±0.27	3.3±1.0	4	4.0±4.0
$\ell\tau\tau$	29.6±5.3	NA	4.9±2.5	0.52±0.19	35.2±5.9	34	24.0±9.1
$\sum \ell(\ell/\tau)(\ell/\tau)$	64±11	1.6±1.6	27±13	5.5±2.1	100±18	111	357±41
$\ell\ell\ell\ell$	0.0000±0.0006	<0.0002	<0.002	0.004±0.001	0.004±0.002	0	18.0±8.2
$\ell\ell\ell\tau$	0.00±0.07	<0.004	<0.02	0.023±0.007	0.02±0.07	0	11.3±6.6
$\ell\ell\tau\tau$	0.33±0.26	<0.002	<0.08	0.04±0.01	0.48±0.27	0	4.0±4.0
$\sum \ell\ell(\ell/\tau)(\ell/\tau)$	0.33±0.27	0.00±0.00	0.00±0.00	0.07±0.02	0.50±0.28	0	33±11

Table 2: Summary of multilepton observations and expectations by lepton flavor for 2.1 fb^{-1} of luminosity with $H_T > 200$ GeV requirement. Events with Z candidates have been removed.

Selection	N(τ)=0		N(τ)=1		N(τ)=2	
	obs	expected SM	obs	expected SM	obs	expected SM
≥FOUR Lepton Results						
MET>50,H_T >200,noZ	0	0.003 ± 0.002	0	0.01 ± 0.05	0	0.30 ± 0.22
MET>50,H_T >200, Z	0	0.06 ± 0.04	0	0.13 ± 0.10	0	0.15 ± 0.23
MET>50,H_T <200,noZ	1	0.014 ± 0.005	0	0.22 ± 0.10	0	0.59 ± 0.25
MET>50,H_T <200, Z	0	0.43 ± 0.15	2	0.91 ± 0.28	0	0.34 ± 0.15
MET<50,H_T >200,noZ	0	0.0013 ± 0.0008	0	0.01 ± 0.05	0	0.18 ± 0.07
MET<50,H_T >200, Z	1	0.28 ± 0.11	0	0.13 ± 0.10	0	0.52 ± 0.19
MET<50,H_T <200,noZ	0	0.08 ± 0.03	4	0.73 ± 0.20	6	6.9 ± 3.8
MET<50,H_T <200, Z	11	9.5 ± 3.8	14	5.7 ± 1.4	39	21 ± 11
THREE Lepton Results						
MET>50,H_T >200,no-OSSF	2	0.87 ± 0.33	21	14.3 ± 4.8	12	10.4 ± 2.2
MET>50,H_T <200,no-OSSF	4	3.7 ± 1.2	88	68 ± 17	76	100 ± 17
MET<50,H_T >200,no-OSSF	1	0.50 ± 0.33	12	7.7 ± 2.3	22	24.7 ± 4.0
MET<50,H_T <200,no-OSSF	7	5.0 ± 1.7	245	208 ± 39	976	1157 ± 323
MET>50,H_T >200,noZ	5	1.9 ± 0.5	7	10.8 ± 3.3	–	–
MET>50,H_T >200, Z	8	8.1 ± 2.7	10	11.2 ± 2.5	–	–
MET>50,H_T <200,noZ	19	11.6 ± 3.2	64	52 ± 13	–	–
MET<50,H_T >200,noZ	5	2.0 ± 0.7	24	26.6 ± 3.3	–	–
MET>50,H_T <200, Z	58	57 ± 21	47	44.1 ± 7.0	–	–
MET<50,H_T >200, Z	6	8.2 ± 2.0	90	119 ± 14	–	–
MET<50,H_T <200,noZ	86	82 ± 21	2566	1965 ± 438	–	–
MET<50,H_T <200, Z	335	359 ± 89	9720	7740 ± 1698	–	–
Totals 4L	13.0	10.4 ± 3.8	20.0	7.8 ± 1.5	45	30 ± 12
Totals 3L	536	539 ± 94	12894	10267 ± 1754	1086	1291 ± 324

Table 3: Results from 2.1 fb^{-1} of 2011 data summed over electron and muon flavors. The labels going down the side refer to whether or not there are OSSF pairs, whether or not $Z \to \ell^+\ell^-$ was excluded (noZ), and the H_T and MET requirements. Labels along the top of the table give the number of τ candidates, 0, 1, or 2. All channels are exclusive. The τ channels serve as "signal" channels for SUSY signals assuming high tan(β) values, for example.

Source of Uncertainty	Uncertainty
Luminosity	4.5%
PDF	14%
Renormalization Scale	10%
Muon ID	0.1 %
Electron ID	0.3%
τ ID	3.7 %
Muon isolation at 8 (100) GeV/c	11% (0.2%)
Electron isolation at 8 (100) GeV/c	14% (0.6%)
Single Muon trigger efficiency	0.5%
Single Electron trigger efficiency	0.7%
Double Muon trigger efficiency	2.5%
Double Electron trigger efficiency	2%
Electron-Muon trigger efficiency	3.7%
$t\bar{t}$ background	50%
WZ background	40%
ZZ background	40%

Table 4: The sources of systematic uncertainties associated with this analysis. Note that the impact of these uncertainties on the result is not necessarily in proportion to their listed values.

"trilepton" signature of supersymmetry in more detail in Fig. 6.

We observe one four-lepton high MET, low H_T event in a bin with a low SM-background expectation. We find that the dominant *a-priori* SM contribution to the bin is from di-Z production, where one of the Z bosons is off-shell. The background estimate is calculated with MADGRAPH, and an uncertainty of 40% is assigned based on differences in the estimate with MCFM [28]. Consistent predictions in control samples of the data that are on-shell or populate regions of phase space yielding low-p_{T} decay products are found; however, data is not available with which to test the MC prediction for off-shell diboson production when the decay products have high-p_{T}.

6.1 Systematic uncertainties and statistical procedures

We discuss the sources of systematic uncertainty and how they impact the search sensitivity before extracting upper limits on the contributions from physics outside the SM. Table 4 lists the salient systematic effects and the resultant uncertainties. All channels share systematic uncertainties for luminosity, renormalization scales, parton distribution functions, and trigger efficiency. The precision of lepton selection efficiencies increases with lepton p_{T}. For a typical slepton co-NLSP signal scenario which has leptons with p_{T} in excess of 20 GeV/c, the lepton identification and isolation efficiency systematic uncertainty is $\sim$ 1.5% per lepton. However, CMSSM signals result in lower p_{T} leptons, leading to a higher systematic uncertainty for the efficiency of $\sim$ 3% per lepton.

We utilize the broad agreement between the expected SM backgrounds and observations to constrain new physics scenarios. The statistical model for the number of events in each channel is a Poisson distribution with expected value, observed value, and log-normal distributions for nuisance parameters. The significant nuisance parameters are the luminosity uncertainty, trigger efficiency, lepton identification efficiencies and background uncertainties. The expected value in the model is the sum of the signal and the expected backgrounds.

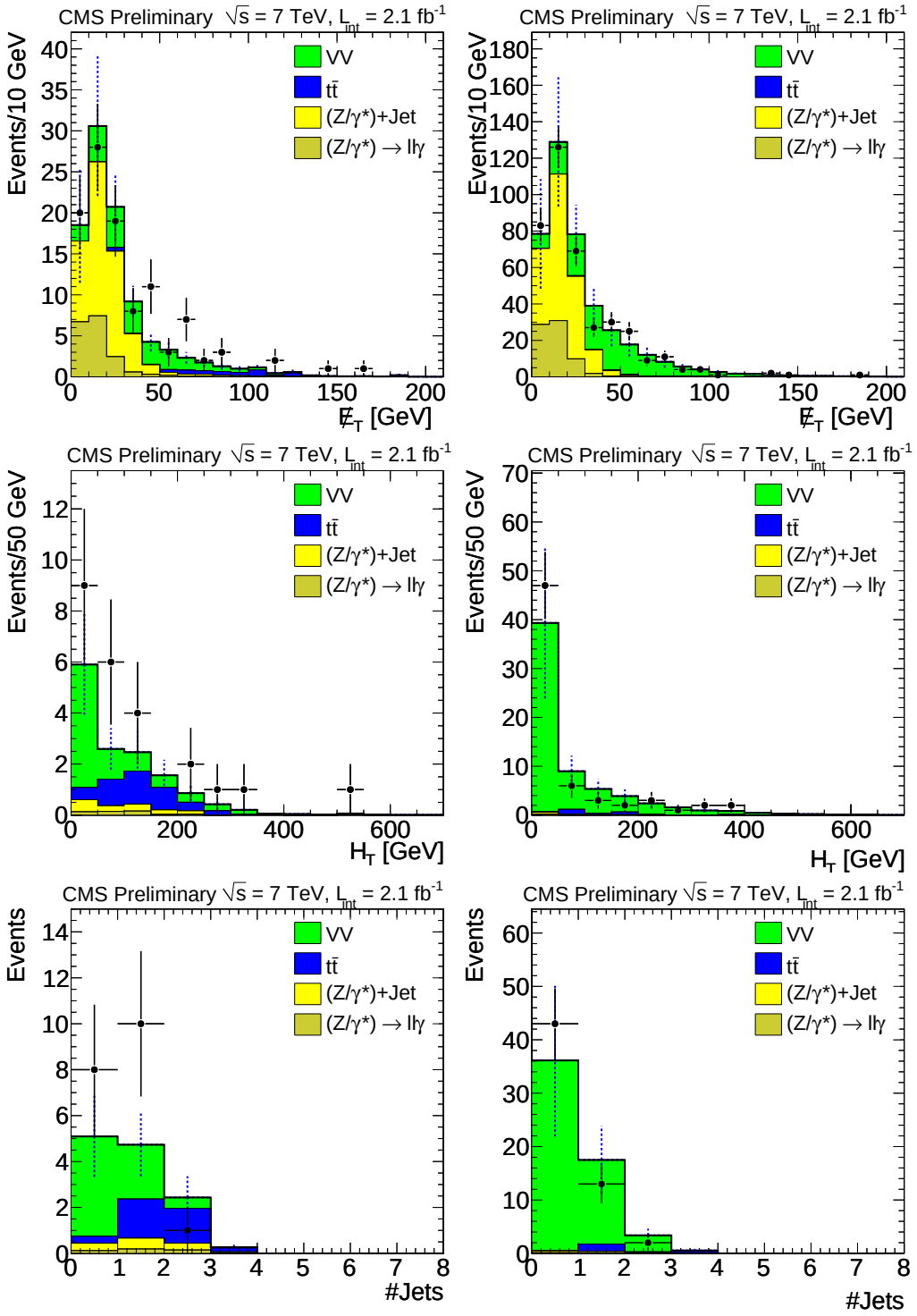

Figure 6: The $E_{\mathrm{T}}^{\mathrm{miss}}$ (top), H_{T} (middle), and jet multiplicity (bottom) distributions for three-lepton events passing all selection criteria, except $E_{\mathrm{T}}^{\mathrm{miss}}$ and H_{T} for the top and middle rows respectively. Observed events (dots with uncertainties) and expected SM background (histogram with dotted uncertainties) are shown. Plots on the left have the Z-veto applied, while plots on the right include leptons from Z decays.

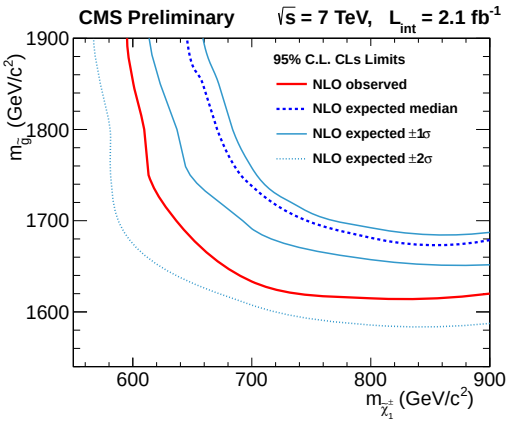

Figure 7: Excluded region in the gluino mass versus wino-like chargino mass plane for the slepton co-NLSP scenario. The region below the red line (observed limit) is excluded at 95% C.L. For comparison the expected limits are shown as well.

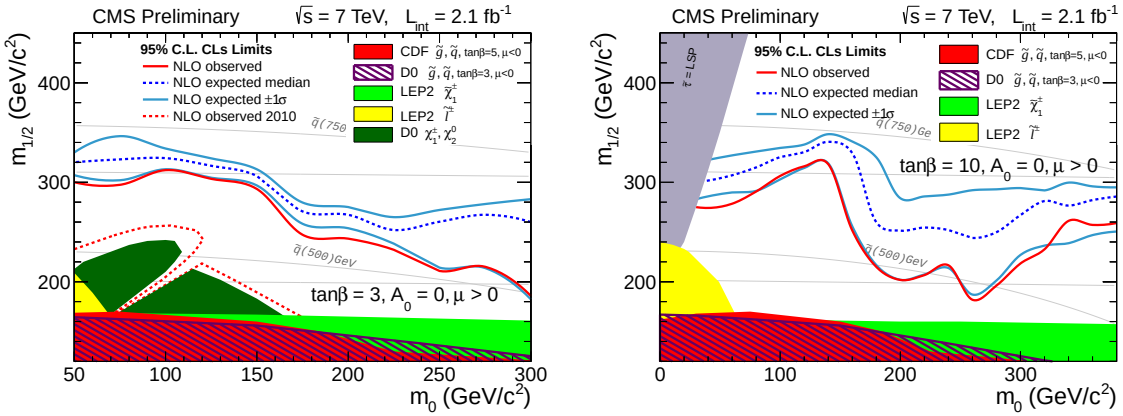

Figure 8: Excluded regions for the CMSSM scenarios with $\tan\beta = 3$ (left) and $\tan\beta = 10$ (right). Values of m_0, $m_{1/2}$ below the red curve (observed limit) are excluded by this analysis. For comparison the expected limits are shown as well.

We set 95% confidence level (C.L.) upper limits on the signal parameters and cross sections using the modified frequentist construction (usually referred to as CLs) [29–31]. We apply these upper limits on the contribution of new physics for the SUSY scenarios outlined below. All cross sections in the following exclusion plots include next-to-leading-order corrections calculated using PROSPINO [32].

6.2 Exclusion in the Slepton co-NLSP Scenario

In supersymmetry, multilepton final states arise naturally in the subset of GMSM parameter space where the right-handed sleptons are flavor-degenerate and at the bottom of the minimal supersymmetric standard model (MSSM) mass spectrum. The Higgsinos are decoupled. Supersymmetric production proceeds mainly through pairs of squarks and/or gluinos. Cascade decays of these states eventually pass sequentially through the lightest neutralino ($\tilde{g}, \tilde{q} \to \chi^0 + X$), which decays into a slepton and a lepton ($\chi^0 \to \tilde{\ell}^{\pm}\ell^{\mp}$). Each of the essentially degenerate right-handed sleptons promptly decays to the Goldstino component of the almost massless and non-interacting gravitino and a lepton ($\tilde{\ell} \to \tilde{G}\ell$) thus yielding events with four or more

hard leptons and missing energy. Such scenarios have a high cross section with little background [16]. The 95% CL exclusion limits for the slepton co-NLSP model is shown in Fig. 7. The exclusion curve asymptotes to the horizontal in regions dominated by strong superpartner production, and to the vertical in regions dominated by weak superpartner production. With strong superpartners decoupled, the production is dominated by wino-like chargino-neutralino and chargino-chargino production, as well as pair production of sleptons with lower masses that are set by the gauge ordered superpartner mass spectra.

6.3 Exclusion in the CMSSM scenario

For the CMSSM [12, 13] scenario, limits in the m_0-$m_{1/2}$ plane are shown in Fig. 8 for $A_0 = 0, \tan\beta = 3, 10$, and $\mu > 0$. They extend significantly the region excluded in our previous analysis [11].

7 Conclusion

We have performed a search for physics beyond the SM using a variety of multilepton final States. We see a good agreement between observations and expectations in channels with large SM expectations both on-Z and off-Z. Taking advantage of the high center-of-mass energy at the LHC, we were able to probe new regions of the MSSM parameter space. Our search complements those at the Tevatron, which are mostly sensitive to electroweak gaugino production via quark-antiquark interaction, while the result presented here is mostly sensitive to gluino and squark production via quark-gluon or gluon-gluon interactions. The results of this search are largely consistent with SM expectations and are used to exclude regions in the MSSM with neutralinos as LSP and co-NLSP scenarios with gravitinos as LSP.

References

[1] H. P. Nilles, "Supersymmetry, Supergravity and Particle Physics", *Phys. Rept.* **110** (1984) 1. doi:10.1016/0370-1573(84)90008-5.

[2] H. E. Haber and G. L. Kane, "The Search for Supersymmetry: Probing Physics Beyond the Standard Model", *Phys. Rept.* **117** (1985) 75. doi:10.1016/0370-1573(85)90051-1.

[3] W. de Boer, "Grand unified theories and supersymmetry in particle physics and cosmology", *Prog. Part. Nucl. Phys.* **33** (1994) 201. doi:10.1016/0146-6410(94)90045-0.

[4] CDF Collaboration, "Search for Supersymmetry in $p\bar{p}$ Collisions at $\sqrt{s}$ = 1.96 TeV Using the Trilepton Signature for Chargino-Neutralino Production", *Phys. Rev. Lett.* **101** (2008) 251801. doi:10.1103/PhysRevLett.101.251801.

[5] S. Dube et al., "Addressing the Multi-Channel Inverse Problem at High Energy Colliders: A Model Independent Approach to the Search for New Physics with Trileptons", (2008). arXiv:0808.1605.

[6] J. T. Ruderman and D. Shih, "Slepton co-NLSPs at the Tevatron", (2010). arXiv:1009.1665.

[7] D0 Collaboration, "Search for associated production of charginos and neutralinos in the trilepton final state using 2.3 fb^{-1} of data", *Phys. Lett.* **B680** (2009) 34. doi:10.1016/j.physletb.2009.08.011.

[8] CDF Collaboration, "Search for Supersymmetry in $p\bar{p}$ Collisions at $\sqrt{s} = 1.96$ TeV Using the Trilepton Signature of Chargino-Neutralino Production", (2009). arXiv:0910.1931.

[9] D0 Collaboration, "Search for R-parity violating supersymmetry via the $LL\overline{E}$ couplings λ_{121}, λ_{122} or λ_{133} in $p\bar{p}$ collisions at $\sqrt{s}$ = 1.96 TeV", *Phys. Lett.* **B638** (2006) 441. doi:10.1016/j.physletb.2006.05.077.

[10] CDF Collaboration, "Search for anomalous production of multilepton events in $p\bar{p}$ collisions at $\sqrt{s}$ = 1.96 TeV", *Phys. Rev. Lett.* **98** (2007) 131804. doi:10.1103/PhysRevLett.98.131804.

[11] CMS Collaboration, "Search for Physics Beyond the Standard Model Using Multilepton Signatures in pp Collisions at sqrt(s)=7 TeV", arXiv:1106.0933.

[12] A. H. Chamseddine, R. Arnowitt, and P. Nath, "Locally Supersymmetric Grand Unification", *Phys. Rev. Lett.* **49** (1982) 970. doi:10.1103/PhysRevLett.49.970.

[13] G. Kane et al., "Study of constrained minimal supersymmetry", *Phys. Rev.* **D49** (1994) 6173. doi:10.1103/PhysRevD.49.6173.

[14] S. Dimopoulos, S. D. Thomas, and J. D. Wells, "Implications of low energy supersymmetry breaking at the Fermilab Tevatron", *Phys. Rev.* **D54** (1996) 3283. doi:10.1103/PhysRevD.54.3283.

[15] SUSY Working Group Collaboration, "Low-scale and gauge-mediated supersymmetry breaking at the Fermilab Tevatron Run II", (2000). arXiv:hep-ph/0008070.

[16] D. Alves et al., "Simplified Models for LHC New Physics Searches", (2011). arXiv:1105.2838.

[17] CMS Collaboration, "Commissioning of the CMS Experiment and the Cosmic Run at Four Tesla", *JINST* **5** (2010) T03001. doi:10.1088/1748-0221/5/03/T03001.

[18] CMS Collaboration, "The CMS experiment at the CERN LHC", *JINST* **3** (2008) S08004. doi:10.1088/1748-0221/3/08/S08004.

[19] GEANT4 Collaboration, "GEANT4: A simulation toolkit", *Nucl. Instrum. Meth.* **A506** (2003) 250. doi:10.1016/S0168-9002(03)01368-8.

[20] F. Maltoni and T. Stelzer, "MadEvent: Automatic event generation with MadGraph", *JHEP* **02** (2003) 027. doi:10.1088/1126-6708/2003/02/027.

[21] T. Sjöstrand, S. Mrenna, and P. Skands, "A Brief Introduction to PYTHIA 8.1", *Comput. Phys. Commun.* **178** (2008) 852. doi:10.1016/j.cpc.2008.01.036.

[22] P. M. Nadolsky et al., "Implications of CTEQ global analysis for collider observables", *Phys. Rev.* **D78** (2008) 013004, arXiv:0802.0007. doi:10.1103/PhysRevD.78.013004.

[23] CMS Collaboration, "Electron Reconstruction and Identification at $\sqrt{s} = 7$ TeV", *CMS Physics Analysis Summary* **CMS-PAS-EGM-10-004** (2010).

[24] CMS Collaboration, "Performance of muon identification in pp collisions at $\sqrt{s} = 7$ TeV", *CMS Physics Analysis Summary* **CMS-PAS-MUO-10-002** (2010).

[25] CMS Collaboration, "Commissioning of the Particle-Flow Reconstruction in Minimum-Bias and Jet Events from pp Collisions at 7 TeV", *CMS Physics Analysis Summary* **CMS-PAS-PFT-10-002** (2010).

[26] CMS Collaboration, "Missing Transverse Energy Performance in Minimum-Bias and Jet Events from Proton-Proton Collisions at $\sqrt{s} = 7$ TeV", *CMS Physics Analysis Summary* **CMS-PAS-JME-10-004** (2010).

[27] CMS Collaboration, "CMS MET Performance in Events Containing Electroweak Bosons from pp Collisions at $\sqrt{s} = 7$ TeV", *CMS Physics Analysis Summary* **CMS-PAS-JME-10-005** (2010).

[28] J. Campbell, R. K. Ellis, and C. Williams, "Vector boson pair production at the LHC", *JHEP* **1107** (2011) 018, arXiv:1105.0020. doi:10.1007/JHEP07(2011)018.

[29] T. Junk, "Confidence Level Computation for Combining Searches with Small Statistics", *Nucl. Instrum. Meth.* **A434** (1999) 435–443, arXiv:hep-ex/9902006. doi:10.1016/S0168-9002(99)00498-2.

[30] A. L. Read, "Modified frequentist analysis of search results (The CL(s) method)",. Prepared for Workshop on Confidence Limits, Geneva, Switzerland, 17-18 Jan 2000.

[31] A. L. Read, "Presentation of search results: The CL(s) technique", *J. Phys.* **G28** (2002) 2693–2704. doi:10.1088/0954-3899/28/10/313.

[32] W. Beenakker, R. Hoepker, and M. Spira, "PROSPINO: A program for the Production of Supersymmetric Particles in Next-to-leading Order QCD", (1996). arXiv:hep-ph/9611232.

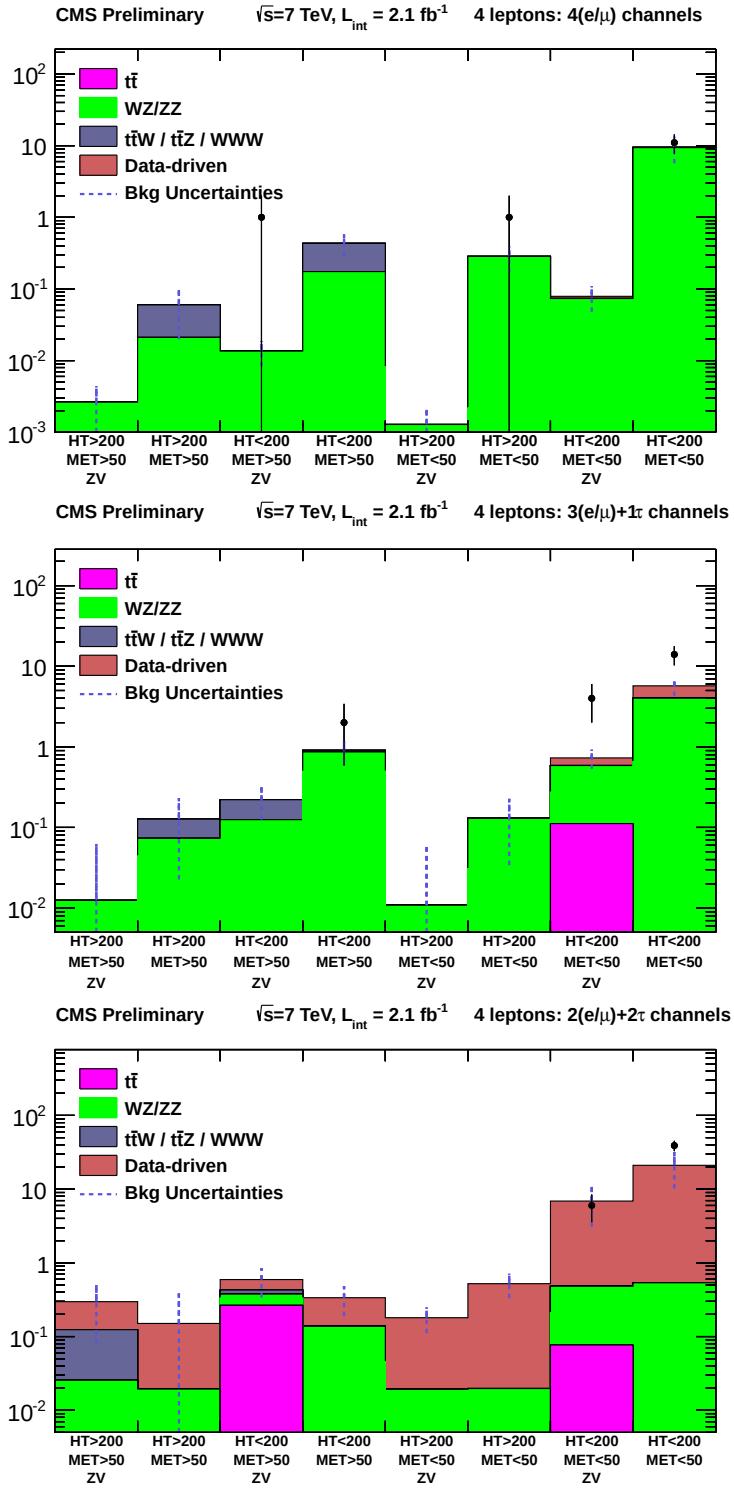

Figure 9: 4-lepton search: Graphical channel-by-channel summaries of the predicted SM backgrounds and observed events in data.

Appendix: Supporting material useful for presentations

Fig. 11 compares the invariant mass of the three leptons measured in data to those obtained

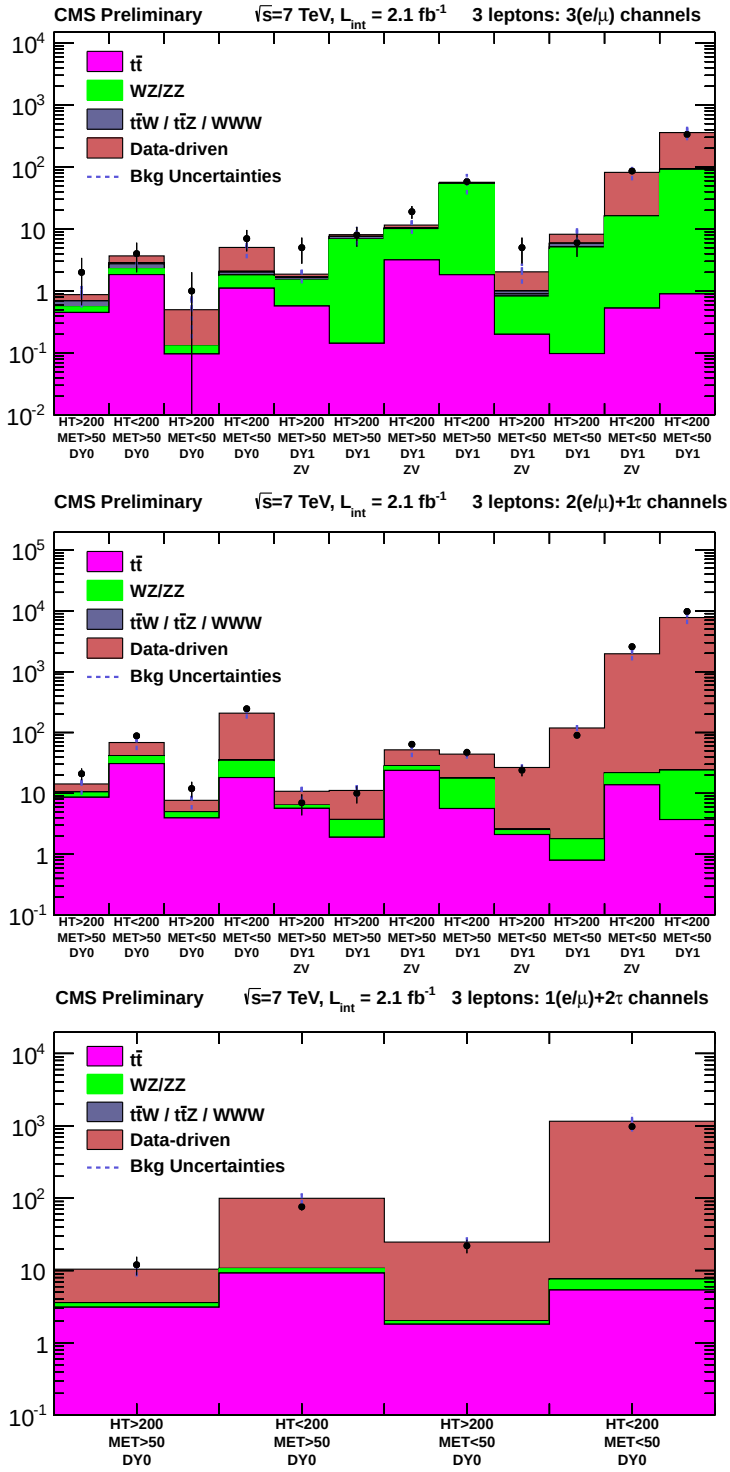

Figure 10: 3-lepton search: Graphical channel-by-channel summaries of the predicted SM backgrounds and observed events in data.

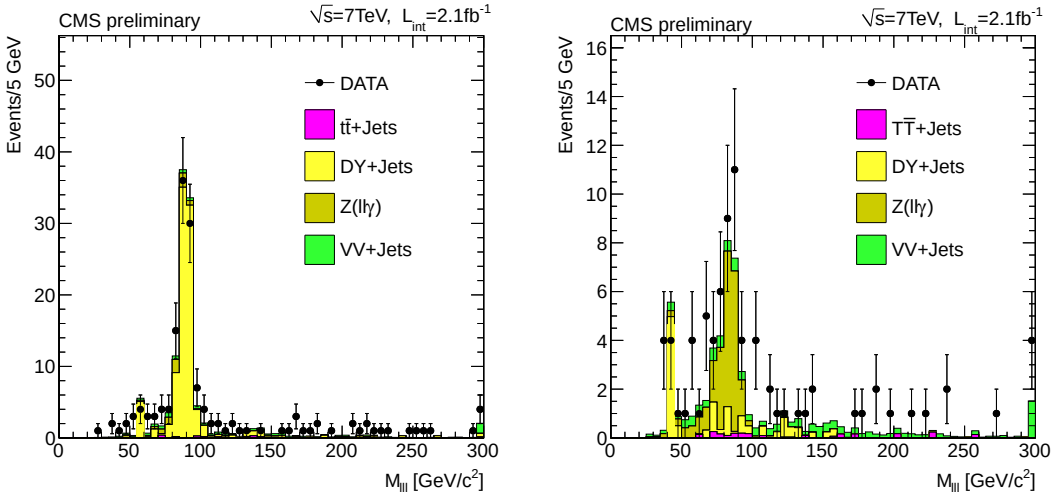

Figure 11: Trilepton invariant mass distributions after a Z veto for OSSF dilepton pairs. Left: $\ell^+\ell^- + e$ channels; right: $\ell^+\ell^- + \mu$ channels. The different contributions for electrons and muons originate for the different probabilities for internal and external conversions , as discussed in the text. Note that the conversion background is estimated using Monte Carlo.

in simulation in events where no OSSF dilepton pair forms an invariant mass of the Z boson. Note the different contributions for electrons and muons. For electrons the third electron originates from final state radiation from the final state electrons. Since muons hardly radiate after production, the main contribution originates from internal pair conversion at the matrix element level. Cuts at the matrix element level may not give the full contribution, since the data is clearly above the prediction in the right panel, thus motivating a data driven measurement of the photon conversion factor described in the main body.